The Phase Envelope of Multicomponent Mixtures in the Presence of a Capillary Pressure Difference

Sandoval Lemus, Diego Rolando; Yan, Wei; Michelsen, Michael Locht; Stenby, Erling Halfdan

Published in:
Industrial and Engineering Chemistry Research

Link to article, DOI:
10.1021/acs.iecr.6b00972

Publication date:
2016

Document Version
Peer-review version

The phase envelope of multicomponent mixtures in the presence of a capillary pressure difference

Diego R. Sandoval, Wei Yan,* Michael L. Michelsen, and Erling H. Stenby

Technical University of Denmark, Kongens Lyngby (Denmark)

E-mail: weya@kemi.dtu.dk

Abstract

Confined fluids such as oil and gas mixtures inside tight reservoirs are systems that can experience high capillary pressure difference between its liquid and gas phase. This capillary pressure difference has an effect on the phase equilibrium and in some cases is considerably high. We presented an algorithm which can reliably compute the whole phase envelope for multicomponent mixtures when there is a capillary pressure difference. It uses an equation of state for the phase equilibrium and the Young-Laplace equation for the capillary pressure model. The algorithm proves to be robust and efficient for test mixtures with a wide range of composition at different capillary radii and vapor fractions. The calculation results show that the phase envelope changes everywhere except at the critical point. The bubble point and the lower branch of the dew point show a decrease in the saturation pressure whereas the upper branch of the dew point shows an increase. The cricondentherm is shifted to a higher temperature. We also presented a mathematical analysis of the phase envelope shift due to capillary pressure based on linear approximations. The resulting linear approximation equations can predict the correct direction of the phase envelope shift. Combined with the multicomponent Clayperon equation, the equations reveal why the shift changes direction for the saturation pressure at the cricondentherm and for

the saturation temperature at the cricondenbar. The equations can be used to estimate the magnitude of shift and the approximation is close for the change in the bubble point pressure.

Introduction

Phase equilibrium in confined spaces is present in many natural systems and industrial applications. One such important example is phase equilibrium in shale, which has received a lot of recent attention due to the shale gas boom. Shale gas production reportedly shows very different trends from conventional gas and oil production. It is speculated by many that shift of the phase equilibrium in the nanoscale pores of shale is one of the major reasons for the abnormal field observations. However, there is no consensus on how phase equilibrium changes in the small pores. It is worthwhile to investigate phase equilibirum in confined spaces more carefully in order to better estimate the initial reserves in shale and better forecast its production.

An important effect in confined space is that the high capillary pressure between the oil and the gas phases can change the bubble or dew point of the system. The effect of capillary pressure on the phase equilibrium has been investigated theoretically and experimentally by several authors. Fisher and Israelachvili[1] confirmed the validity of the Kelvin equation down to a few nanometers ($\approx$ 4nm or eight times the molecular diameter) for pure cyclohexane by measuring liquid bridges between crossed mica cylinders. However, they found it difficult to validate the Kelvin equation when the pressure of the cyclohexane was controlled by adding *n*-dodecane as an involatile solute. This difficulty may be attributed to accumulation of *n*-dodecane in the interface and binary interactions with the cyclohexane in the liquid phase. Multicomponent interactions were addressed by Shapiro and Stenby[2–4] in the formulation of the multicomponent Kelvin equation and its corresponding thermodynamic analysis of multicomponent mixtures under a capillary

pressure difference. In relation to Fisher and Israelachvili's work, Christenson[5] demonstrated the validity of the Laplace equation between water and oil down radii of two nanometers suggesting the validity of continuous curved interfaces at nanometer scale for liquid-liquid systems.

In addition to the effect of the capillary pressure on phase equilibrium, adsorption and confinement play an important role for smaller capillary radii ($\approx$ 2nm). These effects have been investigated for multicomponent mixtures theoretically and through molecular simulations by several authors[6–8] . Our study focuses on the effect of capillary pressure with the smallest capillary radius considered being 5nm. For the matter of this work, the effects of adsorption and confinement are considered negligible in pores above 5nm of radius.

Calculations of saturation pressure and phase envelope for multicomponent mixtures under a capillary pressure difference have been presented by several authors. Brusilovsky[9] presented a simulation of the capillary pressure influence on the dew and bubble point pressures for gas condensate systems. Shapiro and Stenby[4] provided a first-order approximation of the exact solution for the capillary condensation using their Kelvin equation for multicomponent mixtures. They also presented algorithms to solve the flash problem. Nojabaei et al.[10] and Pang et al.[11] calculated the phase envelope in the presence of capillary pressure by solving fugacity equalities coupled with the capillary pressure equation. Both studies show that the phase envelope changes everywhere except at the critical point and at the cricondentherm. They also showed that the change in the saturation pressure is negligible unless the pore radius is on the order of tens of nanometers.

From the viewpoint of computation, saturation point calculation is more difficult than flash calculations.[12] It is recommended to trace the whole phase envelope instead of solving the saturation point problem at an individual temperature or pressure.[12] To the best of our knowledge, no systematic tool or algorithm has been presented to construct the phase envelope for a multicomponent system in the presence of a capillary pressure

difference. In this study we developed such an algorithm that can automatically generate the phase envelope including the quality lines. It provides a reliable tool to study the effect of capillary pressure on the phase envelope at different compositions, capillary radii and vapor fractions. Furthermore, we provided a mathematical analysis that leads to the approximate equations for the shift in saturation pressure/temperature. The equations indicate the same directions of the changes as those from the phase envelope algorithm and explain theoretically why the change happens in various directions.

Methods

The phase envelope calculation algorithm described by Michelsen[13] was employed as the basis for our extension to the calculation with capillary pressure. For phase envelope construction in the presence of capillary pressure several modifications are needed. An obvious modification is to include the capillary pressure equation in the system of equations consisting of equality of fugacity and mass balance shown in (Eq. 1). This results in a computational problem that one of the phase pressures can become negative. Hence, P instead of $\ln P$ is used as the independent variable. The fugacity coefficients at negative pressure are also negative. As a result, it is recommended to use the product of the pressure and its corresponding fugacity coefficient (F_i^α) since the logarithm of fugacity coefficients can also become indefinite. This requires some modifications in the traditional fugacity coefficient based routines in order to get the desired variables and its derivatives at negative pressures.

The system of equations

The system consists of $N_c + 3$ equations, where N_c is the number of components in the mixture. The system has the following form:

$$\begin{cases} \ln K_i + \ln F_i^g(T, P_g, \mathbf{y}) - \ln F_i^l(T, P_l, \mathbf{x}) = 0; \;\; i = 1, ..., Nc \\ \sum_{i=1}^{Nc}(y_i - x_i) = 0 \\ P_l - P_g + P_c(T, P_g, P_l, \mathbf{x}, \mathbf{y}) = 0 \\ X_s - S \end{cases} \tag{1}$$

where:

$$K_i = \frac{y_i}{x_i}, \qquad F_i^\alpha = P^\alpha \varphi_i^\alpha$$

The set of $N_c + 3$ unknown variables are $\mathbf{X} = \left\{\ln K_1, ..., \ln K_{Nc}, \ln T, P_l, P_g\right\}$, where K_i is the equilibrium constant for component i; T is the temperature; P_l is the pressure in the liquid phase; P_g is the pressure in the gas phase; and P_c is the capillary pressure.

The mole fractions x_i and y_i are expressed as a function of the equilibrium constant K_i and feed compositions z_i:

$$x_i = \frac{z_i}{1 - \beta + \beta K_i}, \qquad y_i = \frac{K_i z_i}{1 - \beta + \beta K_i} \tag{2}$$

The last equation of the system in (Eq. 1) is where the desired variable X_s (i.e. $\ln K_i, \ln T, P_g, P_l$) can be specified. The subscript s is the index for the variable to be specified, and S is the desired value of this variable.

The capillary pressure model adopted for our calculations is the Young-Laplace equation:

$$P_c = P_g - P_l = \sigma \left(\frac{1}{R_1} + \frac{1}{R_2} \right) \tag{3}$$

where R_1 and R_2 are the main curvature radii of the curved interface, and σ is the interfacial

tension. Moreover, we assume that the porous media can be represented by capillary tubes of uniform diameter, and that liquid is the wetting phase. The equation (Eq. 3) can be simplified to

$$P_c = P_g - P_l = \frac{2\sigma \cos\theta}{r_c} \tag{4}$$

where θ is the contact angle between the wetting phase and the wall of the tube, and r_c is the capillary radius. For our case, complete wetting was also assumed (i.e. $\theta = 0$).

There exist several models to compute the interfacial tension for mixtures, and the one considered in this study is an extension of the Macleod[14] and Sugden[15] equation:

$$\sigma^{1/E} = \chi(\rho^l - \rho^g) \tag{5}$$

where E is the critical scaling exponent, χ is the parachor constant for each component and ρ^l and ρ^g are the densities of each phase. For (Eq. 5) the units of ρ are $\left(\frac{\text{mol}}{\text{cm}^3}\right)$ and of σ are $\left(\frac{\text{mN}}{\text{m}}\right)$, corresponding to parachor units of $\left(\frac{\text{cm}^3}{\text{mol}}\right)\left(\frac{\text{mN}}{\text{m}}\right)^{\frac{1}{4}}$.

The modified equation for multicomponent mixtures was presented by Weignaug and Katz:[16]

$$\sigma^{1/E} = \sum_{i=1}^{Nc} \chi_i (x_i \rho^l - y_i \rho^g) \tag{6}$$

Different scaling exponents and parachor values can be found in the literature.[16–20] In our methodology we used a critical scaling exponent of $E = 4$ for computational convenience. The parachor values were taken from Schechter and Guo (Table 2 of Ref.[20]).

Solution Approach

The first point is calculated at low gas pressure without taking into account a capillary pressure difference (i.e. $P_l = P_g$) using the algorithm proposed by Michelsen.[13] After we have the first point converged, we estimate the capillary pressure and update the pressure in the liquid phase. At this stage we can switch to the complete system in (Eq. 1) and

start tracing the phase envelope in a sequential way. For each individual point Newton's method was used:

$$\mathbf{X}_{n+1} = \mathbf{X}_n - \mathbf{J}^{-1}\mathbf{f}(\mathbf{X}) \tag{7}$$

where $\mathbf{J}$ is the Jacobian matrix. After convergence, sensitivity analysis is performed to select the appropriate specification variable (S) for the next step. To get the rate of change of the independent variables with respect to the specified one, it is necessary to differentiate (Eq. 1) with respect to S and solve the corresponding system:

$$\mathbf{J}\frac{\partial \mathbf{X}}{\partial S} = -\frac{\partial \mathbf{f}}{\partial S} \tag{8}$$

In our formulation, the pressures in both phases (P_g, P_l) are the only variables that are not in a logarithmic scale. For a proper comparison in the sensitivities, the derivatives were converted to approximate the sensitivity in a logarithmic sense:

$$\frac{\partial \ln P}{\partial S} = \frac{\partial \ln P}{\partial P}\frac{\partial P}{\partial S} = \frac{1}{|P|}\frac{\partial P}{\partial S} \tag{9}$$

To avoid singularities at $P = 0$,

$$\frac{\partial \ln P}{\partial S} \approx \left(\frac{1}{1 + |P|}\right)\frac{\partial P}{\partial S} \tag{10}$$

This scaled sensitivity is more suitable to make a fair comparison within the rest of variables that are logarithmically scaled.

Analysis of the phase envelope shift

Several previous studies[9–11] have calculated the change of saturation pressure due to capillary pressure. However, to the best of our knowledge, there is little discussion on why saturation pressure/temperature changes in different directions in different parts of the

phase envelope. In this section, we aim to provide an analysis showing how to determine the direction of change based solely on the information of the phase equilibrium without capillary pressure. The obtained approximation equations can also be used for quantitative estimates of the change in phase envelope as will be shown in a later section. This analysis was somewhat inpired by the work of Shapiro and Stenby[2] on the multicomponent Kelvin equation.

Saturation pressure

A detailed mathematical analysis for the shift in the **bubble point** pressure is given here. Let us consider any point in the bubble point curve without any capillary pressure difference. At a fixed temperature the point will satisfy the following equation:

$$\ln f_i^l(P_b, \mathbf{z}) = \ln f_i^g(P_b, \mathbf{y_b}), \quad (i = 1, ..., N_c) \tag{11}$$

where f_i^α is the fugacity of component i in phase α, P_b is the normal bubble point pressure, $\mathbf{z}$ is the molar feed composition and $\mathbf{y_b}$ is the molar composition in the incipient gas phase. If we consider a system at a constant temperature confined to a very small capillary pressure difference ($\delta P_c = P_g - P_l$), the bubble point pressure will change accordingly ($\epsilon_p = P_l - P_b$), as well as the molar fraction in the gas phase ($\boldsymbol{\epsilon_y} = \mathbf{y} - \mathbf{y_b}$). Thus the new equilibrium point satisfying the capillary pressure difference (δP_c) is:

$$\ln f_i^l(P_l, \mathbf{z}) = \ln f_i^g(P_g, \mathbf{y}) \tag{12}$$

which can be written as a function of the normal bubble point pressure (P_b) and composition ($\mathbf{y_b}$):

$$\ln f_i^l(P_b + \epsilon_p, \mathbf{z}) = \ln f_i^g(P_b + [\epsilon_p + \delta P_c], \mathbf{y_b} + \boldsymbol{\epsilon_y}) \tag{13}$$

Approximating each term with a linear expansion we get:

$$\begin{aligned}\ln f_i^l(P_b+\epsilon_p,\mathbf{z}) &\approx \ln f_i^l(P_b,\mathbf{z}) + \frac{\partial \ln f_i^l(P_b,\mathbf{z})}{\partial P}\epsilon_p \\ &\approx \ln f_i^l(P_b,\mathbf{z}) + \frac{\bar{V}_i^l}{RT}\epsilon_p \end{aligned} \tag{14}$$

$$\begin{aligned}\ln f_i^g(P_b+[\epsilon_p+\delta P_c],\mathbf{y_b}+\boldsymbol{\epsilon_y}) \approx \ln f_i^g(P_b,\mathbf{y_b}) + \frac{\bar{V}_i^g}{RT}(\epsilon_p+\delta P_c) + \\ + \sum_{j=1}^{N_c}\frac{\partial \ln f_i^g(P_b,\mathbf{y_b})}{\partial y_j}\epsilon_{y_j}\end{aligned} \tag{15}$$

where $\bar{V}_i^\alpha$ is the partial molar volume of component i in phase α, and R is the gas constant. Replacing (Eq. 14-15) in (Eq. 13) and using (Eq. 11) we obtain:

$$\frac{\bar{V}_i^l}{RT}\epsilon_p \approx \frac{\bar{V}_i^g}{RT}(\epsilon_p+\delta P_c) + \sum_{j=1}^{N_c}\frac{\partial \ln f_i^g(P_b,\mathbf{y_b})}{\partial y_j}\epsilon_{y_j} \tag{16}$$

Multiplying (Eq. 16) by the individual molar fraction (y_{b_i}) and summing over all the components i from 1 to N_c we get:

$$\epsilon_p\sum_{i=1}^{N_c} y_{b_i}\bar{V}_i^l \approx V^g(\epsilon_p+\delta P_c) + RT\sum_{i=1}^{N_c}\sum_{j=1}^{N_c} y_{b_i}\frac{\partial \ln f_i^g(P_b,\mathbf{y_b})}{\partial y_j}\epsilon_{y_j} \tag{17}$$

At constant pressure (P) and temperature (T) we can substitute the last term of the right hand side with:

$$RT\sum_{i=1}^{N_c}\sum_{j=1}^{N_c} y_{b_i}\frac{\partial \ln f_i^g(P_b,\mathbf{y_b})}{\partial y_j}\epsilon_{y_j} = \sum_{j=1}^{N_c}\sum_{i=1}^{N_c} y_{b_i}\frac{\partial \mu_i^g(P_b,\mathbf{y_b})}{\partial y_j}\epsilon_{y_j} \tag{18}$$

where μ_i^α is the chemical potential of component i in phase α. This term vanishes due to

the Gibbs-Duhem equation:

$$\sum_{i}^{N_c} y_i \, d\mu_i = 0 \tag{19}$$

Hence our approximation takes the form of:

$$\epsilon_p \sum_{i=1}^{N_c} y_{b_i} \bar{V}_i^l \approx V^g(\epsilon_p + \delta P_c) \tag{20}$$

Replacing the left hand side by the so-called mixed volume[2] :

$$\sum_{i=1}^{N_c} y_{b_i} \bar{V}_i^l = V^{l_g} \tag{21}$$

Consequently we arrive at our final expression:

$$\epsilon_p \approx \delta P_c \left[\frac{V^g}{V^{l_g} - V^g} \right] \tag{22}$$

where V^α is the volume of phase α. Considering our definition of capillary pressure ($P_c = P_g - P_l$) and assuming that our system is a liquid wet capillary tube, the capillary pressure is positive ($\delta P_c > 0$). Hence the direction of the change in the bubble point is indicated by the sign of the dimensionless term $\left[\frac{V^g}{V^{l_g} - V^g} \right]$. A positive value of this term suggests an increase in the bubble point pressure while a negative value suggests a decrease of it.

The **dew point** analysis can be treated similar to the bubble point analysis. At a dew point without capillary pressure we have the condition of equilibrium as follows:

$$\ln f_i^l(P_d, \mathbf{x_d}) = \ln f_i^g(P_d, \mathbf{z}) \tag{23}$$

When there is a small capillary pressure difference ($\delta P = P_g - P_l$), the equilibrium

condition becomes:

$$\ln f_i^l(P_l, \mathbf{x}) = \ln f_i^g(P_g, \mathbf{z}) \tag{24}$$

which leads to a small change in the dew point pressure ($\epsilon_p = P_g - P_d$) and can be written in the following form:

$$\ln f_i^l(P_d + [\epsilon_p - \delta P_c], \mathbf{x_d} + \boldsymbol{\epsilon_x}) = \ln f_i^g(P_d + \epsilon_p, \mathbf{z}) \tag{25}$$

Each term is linearly expanded, and following the same procedure as in the bubble point region we arrive at:

$$\epsilon_p \approx \delta P_c \left[\frac{V^l}{V^l - \sum_{i=1}^{N_c} x_{d_i} \bar{V}_i^g} \right] = \delta P_c \left[\frac{V^l}{V^l - V^{gl}} \right] \tag{26}$$

An equivalent form of this equation was presented by Shapiro and Stenby[3i]. Similar to the bubble point criterion, the direction of the change in the dew point is indicated by the sign of the term $\left[\frac{V^l}{V^l - V^{gl}}\right]$. The above analysis can be generalized to any type of saturation point. The analysis would be done using feed phase and incipient phase instead of specifying in which part of the phase envelope the analysis is being done. The general criterion would be:

$$\epsilon_p \approx -(P^{incp} - P^{feed}) \left[\frac{V^{incp}}{\sum_{i=1}^{N_c} w_i \left(\bar{V}_i^{incp} - \bar{V}_i^{feed} \right)} \right] \tag{27}$$

where (^{incp}) refers to the incipient phase, and w_i is the molar composition of component i in the incipient phase.

[i]Refer to Eq. 11 in the cited article. $P_c = P_d \left(\frac{V_{gl}}{V_l} - 1 \right) P_d(\chi - 1)$ with $\chi = P_g / P_d$

Saturation Temperature

A similar analysis to the saturation pressure can be performed for the saturation temperature. This analysis is particularly useful to explain the shift of cricondentherm in the dew point branch. Instead of fixing the temperature, the pressure in the feed phase will be held constant. This means that ($P_d = P_g$), ($P_l = P_g - \delta P_c$), and lastly ($T_d = T + \epsilon_t$), where T_d is the dew point temperature. The new saturation point of the mixture will satisfy the following equation.

$$\ln f_i^l(P_d - \delta P_c, T + \epsilon_t, \mathbf{x_d} + \boldsymbol{\epsilon_x}) = \ln f_i^g(P_d, T + \epsilon_t, \mathbf{z}) \tag{28}$$

Following the same procedure by expanding linearly each term and summing over the liquid individual compositions x_{d_i}, we arrive at:

$$\epsilon_t = \frac{V^l \delta P_c}{RT \sum_{i=1}^{N_c} x_{d_i} \left(\frac{\partial \ln f_i^l\,(Pd, T, \mathbf{x_d})}{\partial T} - \frac{\partial \ln f_i^g\,(Pd, T, \mathbf{z})}{\partial T} \right)} = -\frac{V^l \delta P_c}{\sum_{i=1}^{N_c} x_{d_i} \left(\bar{S}_i^l - \bar{S}_i^g \right)} \tag{29}$$

where $\bar{S}_i^\alpha$ is the partial molar entropy of component i in phase α. Using an analogous term for the mixed entropy as in the mixed volume.

$$\sum_{i=1}^{N_c} x_{d_i} \bar{S_i^g} = S^{gl} \tag{30}$$

We arrive at our final expression:

$$\epsilon_t = \left[\frac{V^l}{S^{gl} - S^l} \right] \delta P_c \tag{31}$$

where S^α is the entropy of phase α. Once more, the sign of the term $\left[\frac{V^l}{S^{gl} - S^l}\right]$ will indicate the direction of the temperature shift. A similar analysis can be done in the bubble point. Moreover, this analysis can also be generalized for any saturation temperature as it was

done for the saturation pressure in (Eq. 27). The general criterion would be:

$$\epsilon_t \approx (P^{incp} - P^{feed}) \left[\frac{V^{incp}}{\sum_{i=1}^{N_c} w_i \left(\bar{S}_i^{incp} - \bar{S}_i^{feed} \right)} \right] \tag{32}$$

where w_i is the molar composition of component i in the incipient phase.

Relationship with the multicomponent Clapeyron equation

It is worth noting that the multicomponent Clapeyron equation[12,21] can be used to interpret the phase envelope shift due to capillary pressure at cricondentherm and cricondenbar. The multicomponent Clapeyron equation is less known. Similar to the pure component Clapeyron equation, it depicts how the saturation pressure changes with the temperature, but in this case, for a multicomponent system along the phase boundary. Michelsen[12] presented the multicomponent Clapeyron equation in the following form:

$$\frac{dP}{dT} = -\frac{\sum_{i=1}^{Nc} w_i \left(\frac{\partial \ln \varphi_i(\mathbf{w})}{\partial T} - \frac{\partial \ln \varphi_i(\mathbf{z})}{\partial T} \right)}{\sum_{i=1}^{Nc} w_i \left(\frac{\partial \ln \varphi_i(\mathbf{w})}{\partial P} - \frac{\partial \ln \varphi_i(\mathbf{z})}{\partial P} \right)} = \frac{\Delta S}{\Delta V} \tag{33}$$

where the superscript (^{incp}) refers to the incipient phase, and w_i is the molar composition of component i in the incipient phase. The form of the above equation is similar to the pure component Clayperon equation but the entropy change and the volume change have a slightly different meaning here. The two terms are given by:

$$\Delta S = \sum_{i=1}^{N_c} w_i \left(\bar{S}_i^{incp} - \bar{S}_i^{feed} \right); \quad \Delta V = \sum_{i=1}^{N_c} w_i \left(\bar{V}_i^{incp} - \bar{V}_i^{feed} \right) \tag{34}$$

ΔV and ΔS are the changes in the system volume and the system entropy, respectively, when an infinitesimal amount of feed phase is moved to the new incipient phase. From (Eq. 27) and (Eq. 32) we can notice that the direction of the change in the saturation pressure

is related to ΔV and the direction of the change in the saturation temperature is related to ΔS. At the cricondentherm, from the multicomponent Clapeyron equation, we obtain:

$$\frac{dT}{dP} = 0 \;\Rightarrow\; \sum_{i=1}^{N_c} w_i \left(\bar{V}_i^{incp} - \bar{V}_i^{feed} \right) = 0 \tag{35}$$

which suggests a change of sign in the volume difference of the system. Therefore, it implies a change of sign in (Eq. 26) which leads to a change in the direction of the saturation pressure shift around the cricondentherm. The same analysis can be done for change in the saturation temperature around the cricondenbar. At the cricondebar, from the multicomponent Clapeyron equation we obtain:

$$\frac{dP}{dT} = 0 \;\Rightarrow\; \sum_{i=1}^{N_c} w_i \left(\bar{S}_i^{incp} - \bar{S}_i^{feed} \right) = 0 \tag{36}$$

which suggests a change of sign in the entropy difference of the system. Therefore, it implies a change of sign in (Eq. 31) which also leads to a change in the direction of the saturation temperature shift around the cricondenbar. These changes can be confirmed numerically in our later calculations.

Results and discussion

The Soave-Redlich-Kwong Equation of State (SRK EoS) has been used in all the calculations but the calculation can be coupled with any EoS. The proposed algorithm was able to handle all the tested systems at all the specified conditions. The systems tested in this work are: a binary C_1-C_4 system; a 7-component natural gas system; and a set of reservoir fluids with different Gas Oil Ratios (GOR). The algorithm shows to be robust and and quadratically convergent. Typically, we can expect between 2 and 3 iterations per point, and between 20 and 30 points to trace the whole phase envelope.

Before a more detailed analysis, it is helpful to highlight some general features of the

change of the phase envelopes tested here. We used the specific example of System (I) described in Table 1 to illustrate these differences . Figure 1 shows the phase envelope of System (I), and Table 2 shows the values of the pressure and interfacial tension of each point highlighted in the corresponding phase envelope.

Table 1: System I. Natural gas mixture, description of basic model parameters including non zero binary interaction parameters (k_{ij})

Component	mol %	parachor (χ)	P_c (bar)	T_c (K)	ω	$k_{N_2 j}$	$k_{CH_4 j}$
N_2	1.40	61.12	126.20	34.00	0.0377	0	0.0278
CH_4	94.30	74.05	190.56	45.99	0.0115	0.0278	0
C_2H_6	2.70	112.91	305.32	48.72	0.0995	0.4070	-0.0078
C_3H_8	0.74	154.03	369.83	42.48	0.1523	0.0763	0.0090
nC_4	0.49	193.90	425.12	37.96	0.2002	0.0700	0.0056
nC_5	0.27	236.00	469.70	33.70	0.2515	0.0787	0.0190
nC_6	0.10	276.71	507.60	30.25	0.3013	0.1496	0.0374

Table 2: Values corresponding to highlighted points in Figure 1.

Observation	T (K)	P (bar)	P_l (bar)	P_g (bar)	ΔP_{sat}	ΔP_c	σ (mN/m)
Bubble point [a]	150.00	11.09	-1.26	10.48	-12.35	11.74	5.87
Critical point [b]	203.24	58.94	58.94	58.94	0	0	0.00
Dew point [c]	250.00	73.52	69.92	76.59	3.07	6.67	3.34
Cricondentherm [d]	260.71	38.94	-	-	-		0.00
Cricondentherm [d]	263.37	-	21.61	38.94	-	17.33	8.67
Dew point [e]	250.00	10.94	-18.64	8.66	-2.28	27.3	13.65

In the bubble point branch of the phase envelope, the saturation pressure is suppressed until the critical point is reached. The supression increases with the distance from the critical point. For this part of the phase envelope, the reference pressure is the liquid pressure (P^l). The selection of the reference phase pressure is based on two considerations: first, the liquid phase is the feed phase; second, during a bubble point phase transition, the liquid pressure is the parameter that can be measured before the formation of a gas phase. Graphically, this difference in the saturation pressure is the distance between the black line and the blue dashed line in Figure 1. This behavior can be confirmed by (Eq. 22). If we compute $\left[\frac{V^g}{V^{lg}-V^g}\right]$ for the saturation points belonging to the bubble point curve we can

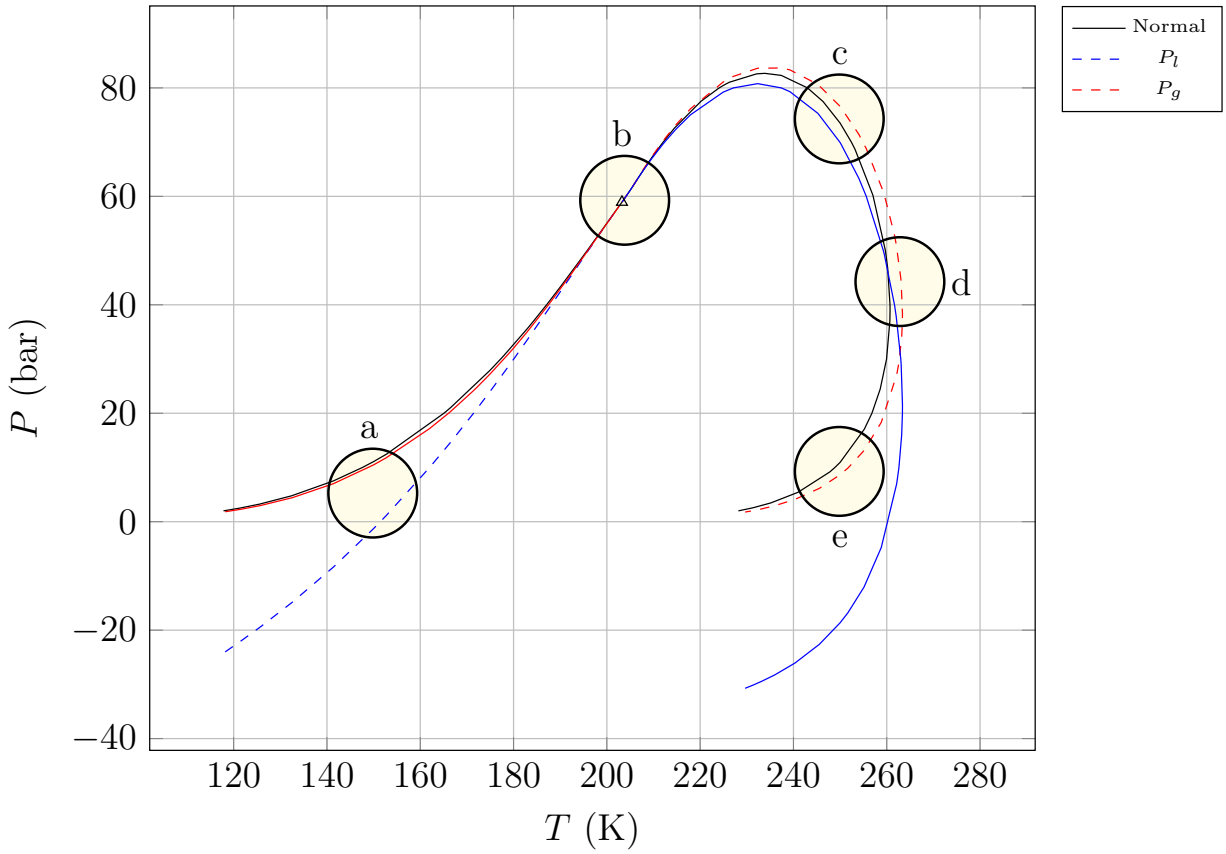

Figure 1: Phase Envelope in the presence of capillary pressure of System (I) using a capillary radius of 10 nm. Highlighted circles show the main differences and similarities with respect the normal phase envelope.

notice that all the values are negative (see Table 3). This suggests a decrease in the bubble point pressure.

The critical point does not show any change because the properties of both phases are indistinguishable and the value for the interfacial tension (σ) given by (Eq. 6) is zero, corresponding to a zero capillary pressure value.

The dew point branch of the phase envelope shows different behaviors depending on which part of it we refer to. The reference pressure in the dew point is the gas phase pressure (P^g). Graphically, this means that the difference in the saturation pressure is the distance between the black line and the red dashed line in Figure 1. Firstly, from the critical point to the cricondentherm, the upper dew point branch, the saturation pressure

Table 3: Direction of change of the saturation pressure in the bubble point region due to a capillary pressure difference in the system.

T (K)	P (bar)	$\frac{V^g}{V^{lg}-V^g}$
110.98	1.22	-1.00
120.74	2.41	-1.01
128.62	3.86	-1.01
139.03	6.69	-1.02
152.64	12.39	-1.03
166.43	21.09	-1.06
177.75	30.65	-1.13
186.52	39.50	-1.26
193.05	46.82	-1.53
202.63	58.20	-16.32

increases; then, the cricondentherm shows a shift to a higher temperature; and finally, from the cricondentherm onwards the saturation pressure is suppressed. The difference in the dew point seems to decrease gradually while lowering the gas pressure and the difference becomes apparently zero at very low pressures.

Again, this behavior can be confirmed by (Eq. 26). Table 4 shows the direction of the pressure change along the dew point region. The sign of these values suggests an increase of the dew point pressure in the upper branch and a decrease in the lower branch. Moreover, at very low pressures this value is close to zero due to big changes in the volume of the incipient phase in comparison with the volume in the feed. It is also important to notice that in Table 4 a change from negative infinity to positive infinity occurs at the cricondentherm. For this reason, to have a clear picture of the behavior around the cricondentherm, the saturation temperature must be analyzed instead of the saturation pressure. The direction of the change in the saturation temperature can be obtained from (Eq. 31). Table 5 shows the direction in the change of the saturation temperature along the dew point curve. The sign of these values confirms the behavior of the temperature increase in the cricondentherm.

The changes of sign in the cricondentherm and cricondenbar for the shift in saturation pressure and saturation temperature shown in Table 4 and Table 5 respectively, are a direct

consequence of the multicomponent Clapeyron equation. From (Eq. 35) and (Eq. 36) we can notice that a change of sign is guaranteed. As a result, ϵ_p and ϵ_t in (Eq .26) and (Eq .31) respectively, change from positive infinity to negative infinity or vice versa.

Table 4: Direction of change of the saturation pressure in the dew point region due to a capillary pressure difference in the system.

T (K)	P (bar)	$\left[\frac{V^l}{V^l - V^{gl}}\right]$
226.51	1.74	-0.01
239.08	4.66	-0.02
247.36	8.76	-0.04
256.85	19.94	-0.12
260.55	33.17	-0.26
257.16	60.46	1.98
245.26	80.33	0.64
236.71	82.39	0.39
229.37	82.03	0.35
214.80	72.92	0.32
207.35	64.30	0.44
203.71	59.50	11.95

Table 5: Direction of change of the saturation temperature in the dew point region due to a capillary pressure difference in the system.

P (bar)	T (K)	$\left[\frac{V^l}{S^{gl} - S^l}\right]$
1.74	226.51	0.088
8.76	247.36	0.107
18.33	256.26	0.124
33.17	260.55	0.148
58.10	258.56	0.213
60.46	257.16	0.226
82.39	236.71	2.002
82.03	229.37	-1.308
78.52	221.71	-0.494
72.92	214.80	-0.347
67.61	209.75	-0.358
60.40	204.45	-9.403

The above general features are observed in all the phase envelopes calculated in this work. These features remain the same as long as the liquid phase is assumed to

be the wetting phase, and the geometry does not change. Moreover, these features are consistent with the results of previous authors with the only difference in the shift of the cricondentherm.[10,11] This difference was probably caused by a numerical artifact in these previous studies due to poor initial estimates. This may have caused difficulties finding solutions in regions that are not present in the normal phase envelope problem. It also shows the necessity of having a robust and efficient algorithm to automatically trace the whole phase envelope in the presence of capillary pressure.

The following subsections present a more detailed discussion regarding the influence of the feed composition composition and capillary radius; and the construction of the quality lines in the phase envelope.

Effect of the feed composition

We refer to this effect as the change in the phase envelope due to a different feed composition. In this subsection, we analyze systems with different feed composition and its changes on the phase envelope.

A set of reservoir fluids with different Gas Oil Ratio (GOR) described in Table 6 were tested. These fluids were taken from Whitson and Sunjerga[22] and were used in mechanistic simulations for liquid rich shale reservoirs. They represent an example of a real confined multicomponent systems. Figure 2 and Figure 3 show the phase envelope of these systems. While the heavier mixtures (low GOR) present a bigger change in the bubble point region, the lighter mixtures (high GOR) present it in the dew point region. Also, the change in the bubble point region is more pronounced in comparison to the one in the dew point region.

These behaviors are intimately related to the density difference between the feed phase and the new incipient phase formed. A bigger difference in the density will create a higher interfacial tension which contributes to a higher capillary pressure difference as it can be seen in (Eq. 6) and (Eq. 4). For the heavier systems, the gas phase formed in bubble point transition will be very light in comparison to the liquid phase, therefore the capillary

pressure will be high. For the dew point transition, the gas phase will contain heavy components and when the liquid phase is formed, the difference in the densities will not be that high. The opposite analysis can be done for the lighter systems.

To have an idea of the magnitude of change in the saturation pressure, Figure 4 shows the changes in the saturation pressure of the different GOR reservoir fluids at the constant temperature of 400 K. It can be noticed that at this temperature the bubble point systems are affected the most. The heavier the system, the higher the change in the saturation pressure. However, this only shows one fixed temperature. In order to have a better picture of what can be expected in reservoirs at different temperatures containing different reservoir fluids, it is necessary to compare changes in a range of temperatures rather than in a fixed temperature. Table 7 shows the maximum change in the saturation pressure for the same set of reservoir fluids in the temperature range of 300 K to 500 K. It can be noticed that the heavy fluids have big negative changes in the bubble point pressure and the lightest have positive changes in the dew point pressure. The shift in the bubble point pressure implies a larger liquid phase region, and the positive shift in the dew point implies a larger upper region for gas condensation. The fluids that lay in the middle have small changes since at those temperatures are near critical fluids.

Table 6: Reservoir fluid systems general description. Taken from Whitson and Sunjerga[22]

GOR (scf/STB)	OGR (STB/MMscf)	STO API	C_7^+ MW (mol/g)	C_7^+ (mol%)
33333	30	51.4	123	3.47
20000	50	49.8	132	4.51
10000	75	47.5	145	7.08
6667	150	46.2	153	9.48
4000	250	44.5	164	13.78
2857	350	43.4	171	17.59
2000	500	42.3	178	22.59
1000	1000	40.0	195	34.88
500	2000	37.7	216	49.49

Table 7: Maximum saturation pressure change for GOR systems in the temperature range of 300 K to 500 K

GOR (scf/STB)	Bubble point (bar)	Dew point (bar)
33333	-	7.38
20000	-	3.53
13333	-0.04	2.76
10000	-0.06	1.37
6667	-0.34	0.52
4000	-1.06	0.01
2857	-2.24	-
2000	-3.79	-
1000	-7.85	-
500	-11.86	-

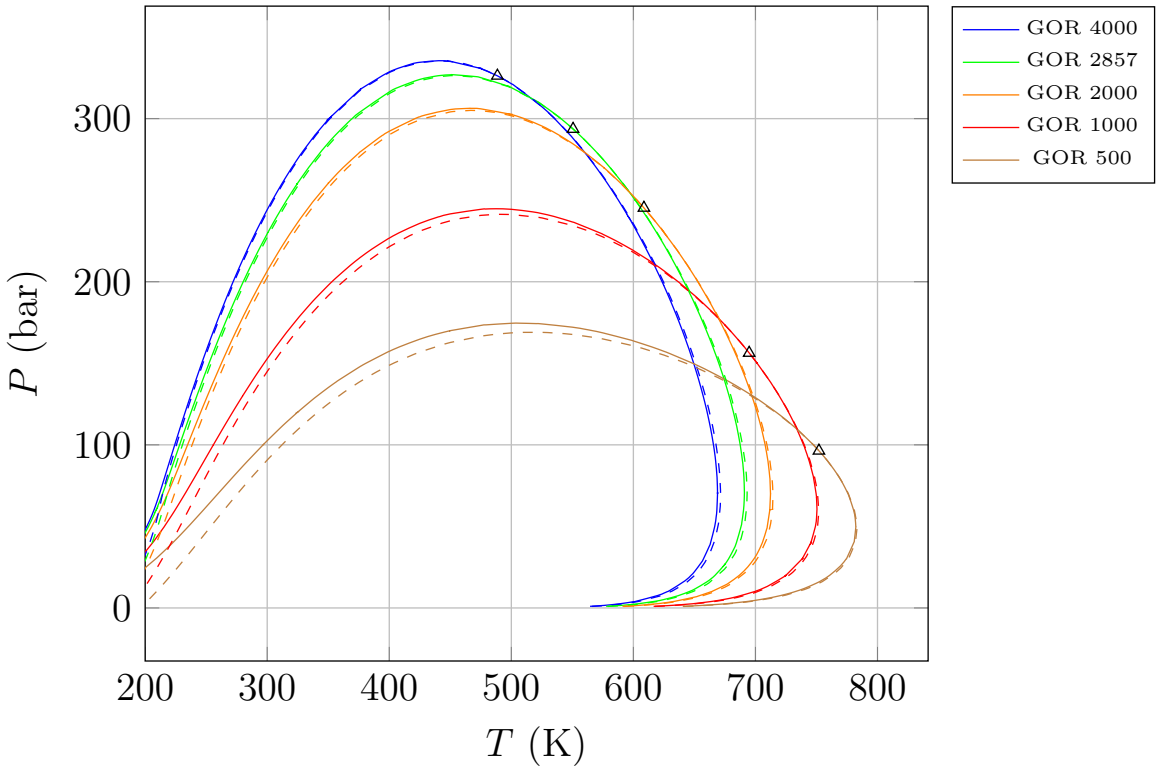

Figure 2: Phase envelope of reservoir fluid mixtures described in Table 6 with GOR ranging from 500 to 4000 scf/STB. The solid lines (—) represent the normal phase envelopes; Dashed lines (- - -) represent the modified phase envelopes due to a capillary pressure difference using r_c = 10nm.

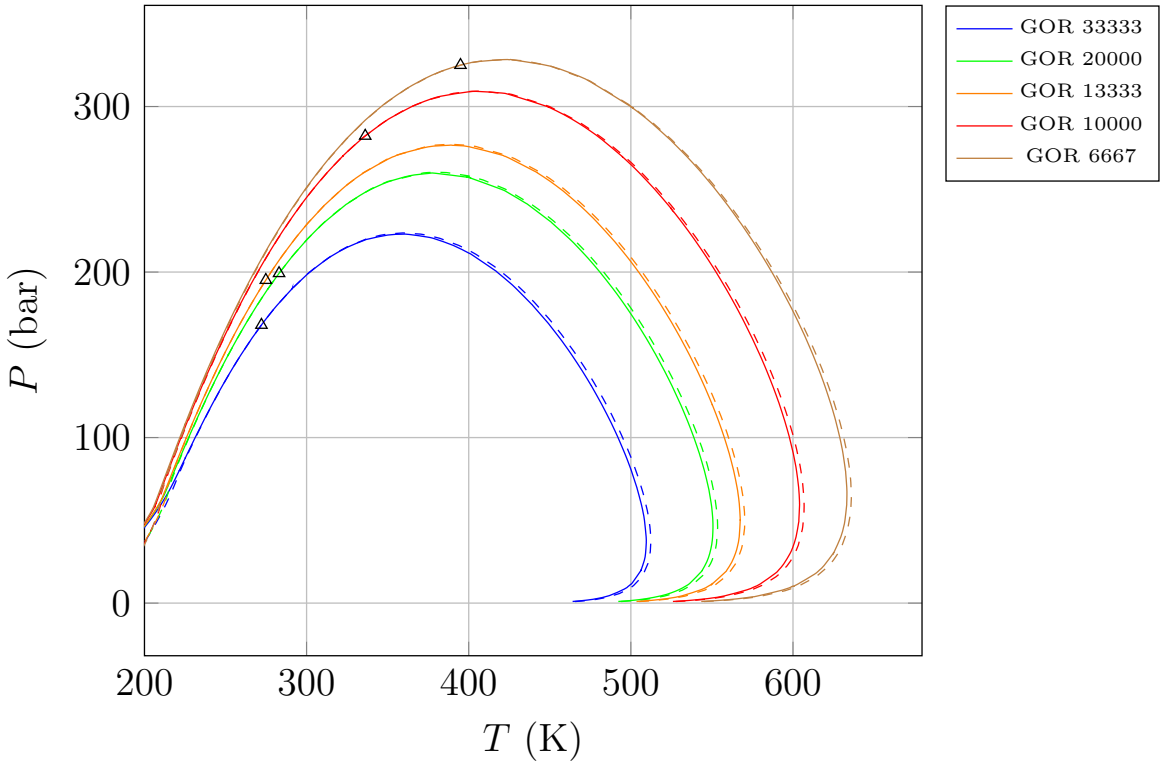

Figure 3: Phase envelope of reservoir fluid mixtures described in Table 6 with GOR ranging from 6667 to 33333 scf/STB. The solid lines (—) represent the normal phase envelopes; Dashed lines (- - -) represent the modified phase envelopes due to a capillary pressure difference using r_c = 10nm.

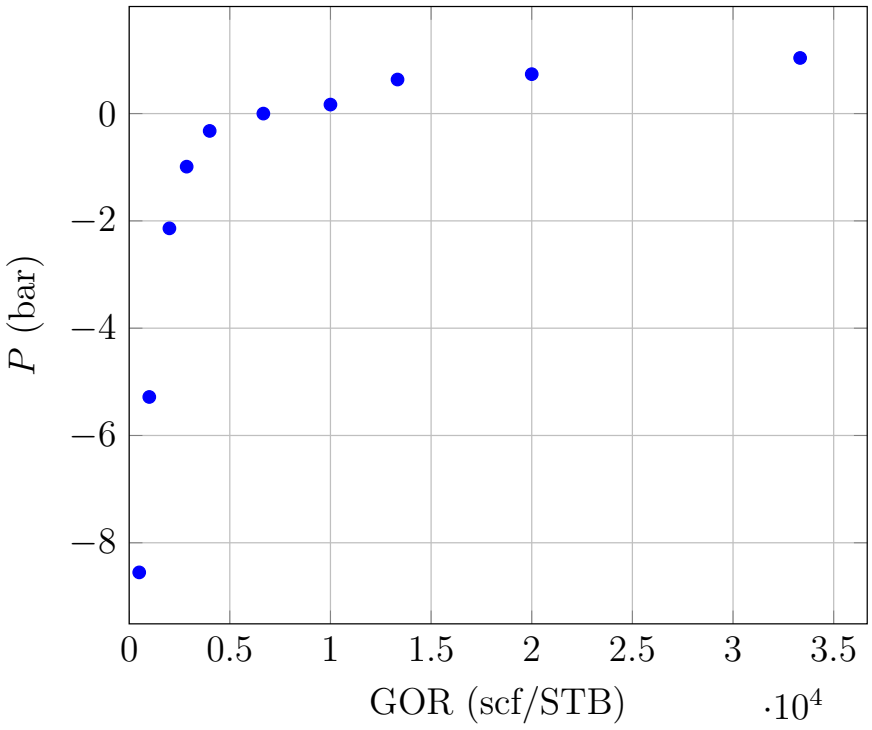

Figure 4: Saturation pressure variation respect GOR at (400 K)

Capillary radius

The effect of the capillary radius on the phase envelope is quite intuitive. At smaller capillary radii the change in the saturation pressure will be increased due to a bigger capillary pressure difference. Figure 5 shows the changes of the saturation pressure at different capillary radii for a C_1-C_4 binary system described in Table 8. Additionally, it is possible to show that the change of the saturation pressure is approximately linear to the inverse of the capillary radius. If we replace (ΔP_c) with $(2\sigma/r_c)$ in (Eq. 22) and (Eq. 26) we obtain that the shift in the saturation pressure can be approximated as a function of the capillary radius.

$$\epsilon_p^{bubble} \approx \frac{2\sigma}{r_c}\left[\frac{V^g}{V^{l_g} - V^g}\right] \quad ; \quad \epsilon_p^{dew} \approx \frac{2\sigma}{r_c}\left[\frac{V^l}{V^l - V^{g_l}}\right] \tag{37}$$

If we plot the real change in the saturation pressure at a constant temperature against the inverse of the capillary radius and compare with the expressions in (Eq. 37) we get very close plots as shown in Figure 6 and Figure 7. Therefore, we can approximate in a realistic way the change of phase envelope at different capillary radii using the linear approximations developed in the previous section. In other words, by having the normal saturation point and the capillary radius, we can obtain an approximation of the shift in the saturation pressure with a simple linear relationship. In many cases, this approximation is sufficiently accurate for the bubble point branch and upper dew point as it can be seen in Figure 6 and Figure 7.

Table 8: Binary system. Description of basic model parameters. ($k_{ij} = 0$)

Component	parachor (χ)	P_c (bar)	T_c (K)	ω
CH_4	74.05	190.56	45.99	0.0115
nC_4	193.9	425.12	37.96	0.2002

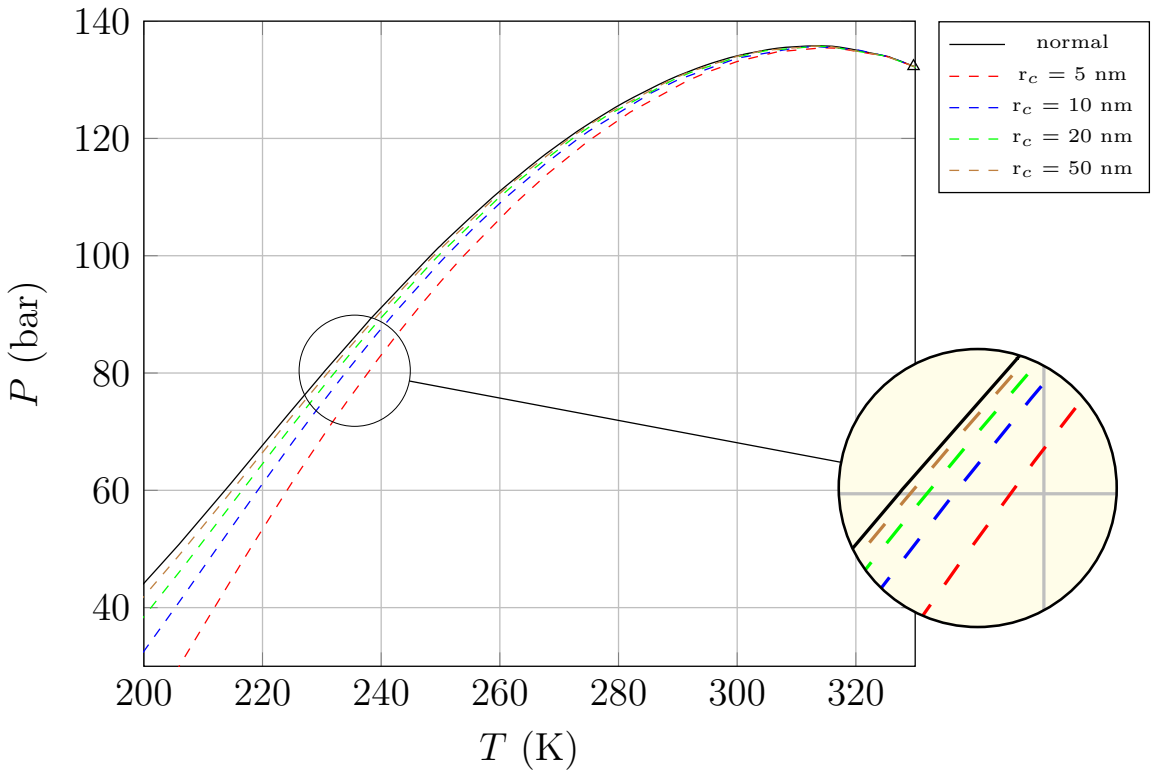

Figure 5: Bubble point change at different capillary radius (r_c) for a 70-30 mol% C_1-C_4 mixture.

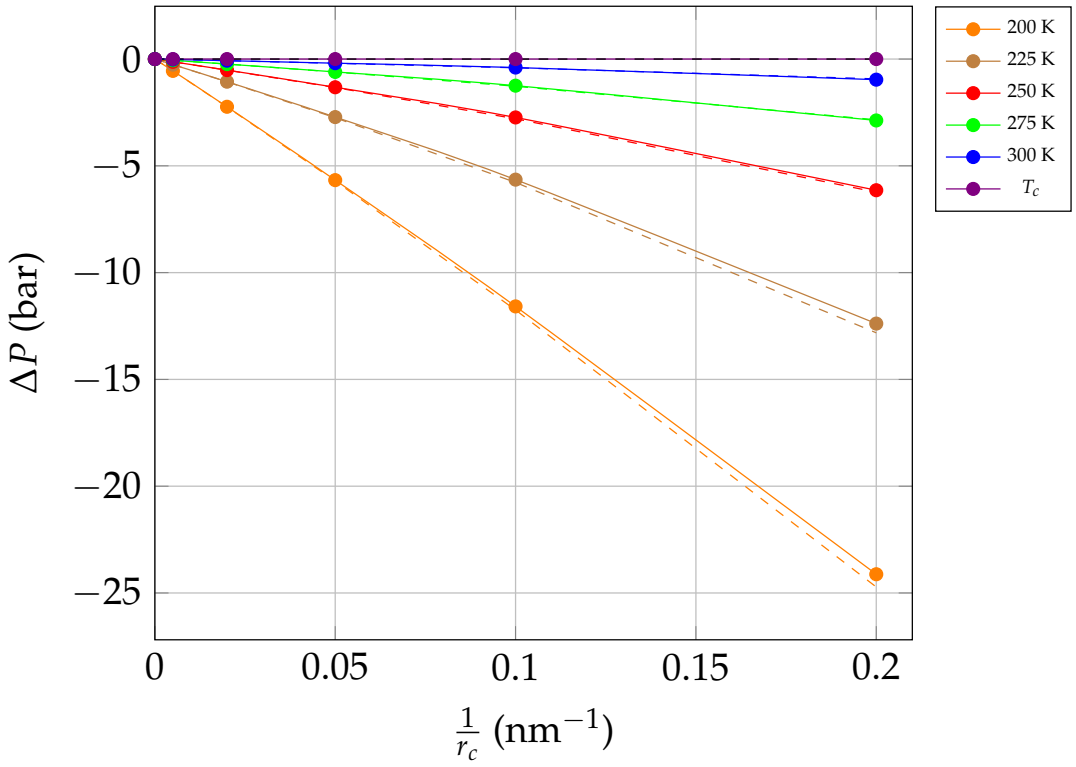

Figure 6: Bubble point change at different temperatures as a function of the inverse of the capillary radius (r_c) for a 70-30 mol% C_1-C_4 mixture. Dashed lines (- - -) show the approximation given by (Eq. 37).

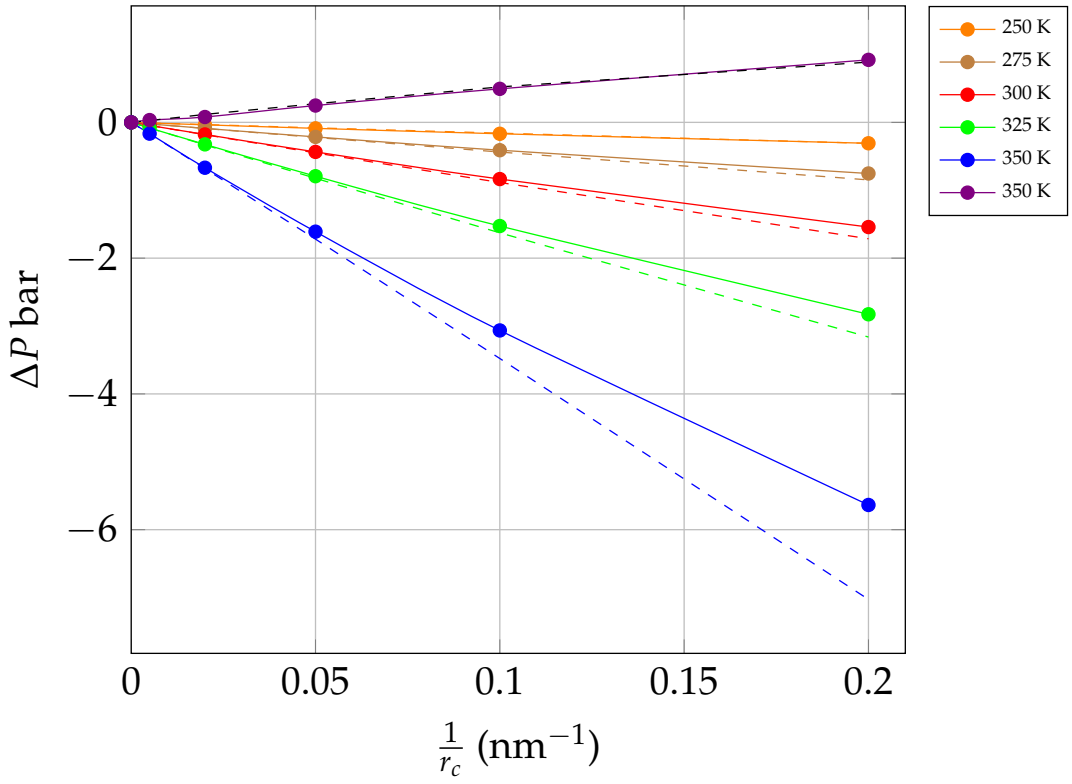

Figure 7: Dew point change at different temperatures as a function of the inverse of the capillary radius (r_c) for a 70-30 mol% C_1-C_4 mixture. Dashed lines (- - -) show the approximation given by (Eq. 37).

Quality lines

A robust phase equilibrium calculation algorithm should also be able to calculate quality lines with $(0 \leq \beta \leq 1)$ in addition to the bubble point curve and the dew point curve. This feature is useful to understand the behavior of multicomponent mixtures in the two-phase region. Figure 8 provides such an example for a C1-C4 mixture. From the figure, one can infer how the liquid phase fraction will change during a constant mass expansion process in the presence of capillary pressure.

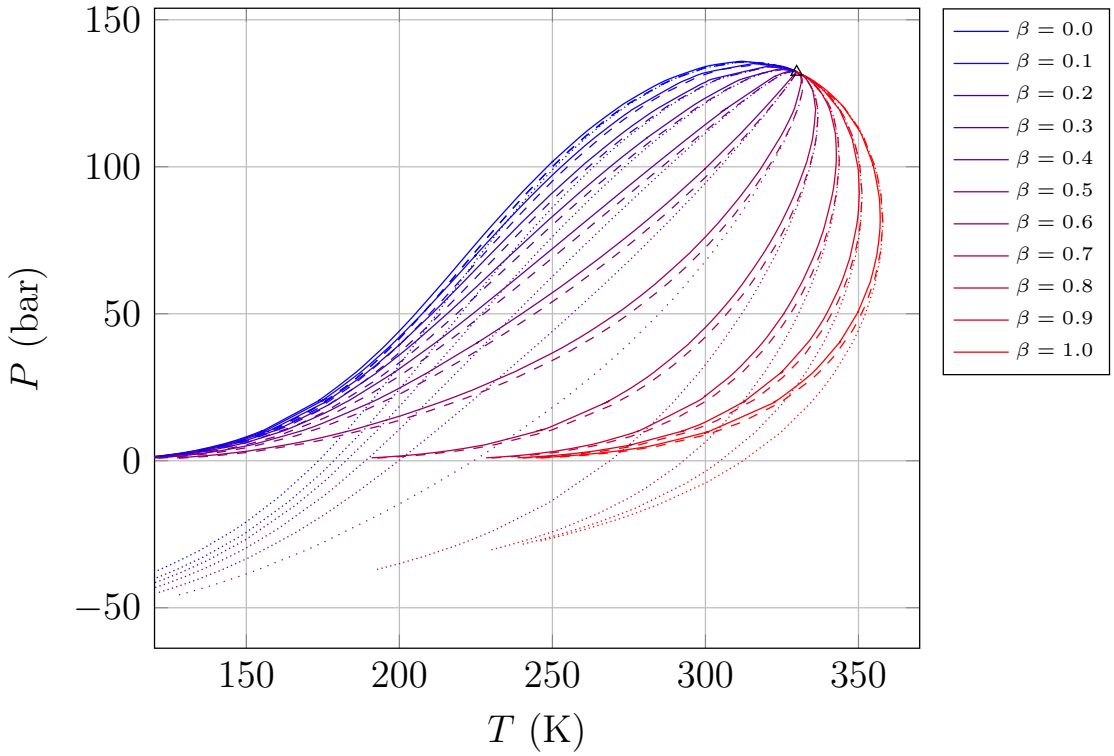

Figure 8: Quality lines at different vapor fractions (β) for a 70-30 mol% C_1-C_4 system. Solid lines (—) represent the normal quality lines; dotted lines (· · ·) the modified P_l and dashed lines (- - -) the modified P_g due to a capillary pressure difference using r_c=10nm

Conclusions

We developed an efficient and robust algorithm that can trace the entire phase envelope of a multicomponent mixture in the presence of capillary pressure. It serves as a useful tool for studying the effect of capillary pressure on phase envelope at different feed compositions, capillary radii and vapor phase fractions.

The algorithm was used to calculate various systems from simple binary mixtures to multicomponent natural gas and reservoir fluids. The results show that capillary pressure shifts the original phase envelope in all the places except the critical point.

The magnitude of saturation pressure change is case dependent. But for the range of capillary radius studied here (larger than 5 nm), the change seems to be moderate. It should be noted that the current analysis assumes just a single pore size and the effect or pore size distribution should be investigated in the future. In addition, the influence of adsorption and confinement should also be taken into account.

We also provided an analysis through linear approximation at the saturation point and derived the equations for the approximate shifts in saturation point in the presence of capillary pressure. The linear approximation equations provide a way to judge the direction of the shift and to estimate the magnitude of the shift based only on the saturation point without capillary pressure. In other words, no saturation point calculation with capillary pressure is needed to use the equations. Our results show that the equations predict the same directions of change as those from the rigorous phase envelope calculation. Moreover, these equations relate the saturation point shift to the change in volume or entropy if an infinitesimal amount of incipient phase is formed, thus providing a physical interpretation for the effect of capillary pressure. In particular, multicomponent Clayperon equation indicates that the volume change is zero at the cricondentherm and the entropy change is zero at the cricondenbar. As a result, the saturation pressure shift and the saturation temperature shift change the direction at these two points, respectively. These linear approximation equations can be used as initial estimates for saturation points, and

in many cases may be sufficiently accurate for bubble point calculation with capillary pressure.

Acknowledgments

The authors acknowledge ConocoPhillips and ExxonMobil for their financial support. We are grateful to Prof. Alexander Shapiro for the valuable discussions.

Supporting Information Available

The following files are available free of charge.

- **Sensitivity Analysis**: Shows a sensitivity analysis of the phase envelope on the interfacial tension (σ) model. In specific, for the scaling exponent (E) and parachors (χ).

This material is available free of charge via the Internet at `http://pubs.acs.org/`.

References

(1) Fisher, L. R.; Israelachvili, J. N. Experimental studies on the applicability of the Kelvin equation to highly curved concave menisci. *Journal of Colloid and Interface Science* **1981**, *80*, 528–541.

(2) Shapiro, A.; Stenby, E. Kelvin equation for a non-ideal multicomponent mixture. *Fluid Phase Equilibria* **1997**, *134*, 87–101.

(3) Shapiro, A.; Stenby, E. Thermodynamics of the multicomponent vapor liquid equilibrium under capillary pressure difference. *Fluid Phase Equilibria* **2001**, *178*, 17–32.

(4) Shapiro, A.; Stenby, E. Effects of Capillary Forces and Adsorption on Reserves Distribution. SPE European Petroleum Conference. Milan, Italy, 1996; pp 441–448.

(5) Christenson, H. Capillary condensation in systems of immiscible liquids. *Journal of Colloid and Interface Science* **1985**, *104*, 234–249.

(6) Zarragoicoechea, G. J.; Kuz, V. a. Critical shift of a confined fluid in a nanopore. *Fluid Phase Equilibria* **2004**, *220*, 7–9.

(7) Singh, S. K.; Sinha, A.; Deo, G.; Singh, J. K. Vapor - Liquid Phase Coexistence, Critical Properties, and Surface Tension of Confined Alkanes. *J. Phyis. Chem. C* **2009**, *113*, 7170–7180.

(8) Travalloni, L.; Castier, M.; Tavares, F. W.; Sandler, S. I. Thermodynamic modeling of confined fluids using an extension of the generalized van der Waals theory. *Chemical Engineering Science* **2010**, *65*, 3088–3099.

(9) Brusilovsky, A. I. Mathematical Simulation of Phase Behavior of Natural Multicomponent Systems at High Pressures With an Equation of State. *SPE* **1992**, *February*, 117–122.

(10) Nojabaei, B.; Johns, R. T.; Chu, L.; Corporation, H. Effect of Capillary Pressure on Phase Behavior in Tight Rocks and Shales. *SPE* **2013**, *August*, 281–289.

(11) Pang, J.; Zuo, J.; Zhang, D.; Du, L.; Corporation, H. IPTC 16419 Effect of Porous Media on Saturation Pressures of Shale Gas and Shale Oil. IPTC. Beijing, China, 2013; pp 26–28.

(12) Michelsen, M.; Mollerup, J. *Thermodynamic models; Fundamentals and Computational aspects*; 1998.

(13) Michelsen, L. Calculation of phase envelopes and critical points for multicomponent mixtures. *Fluid Phase Equilibria* **1980**, *4*, 1–10.

(14) Macleod, D. B. On a relation between surface tension and density. *Trans. Faraday Soc.* **1923**, *19*, 38–41.

(15) Sugden, S. A relation between surface tension, density, and chemical composition. *Journal of the Chemical Society, Transactions* **1924**, *125*, 1177.

(16) Weinaug, C. F.; Katz, D. L. Surface Tensions of Methane-Propane Mixtures. *Industrial and Engineering Chemistry* **1943**, *35*, 239–246.

(17) Hugill, J.; Welsenes, A. V. Surface Tension: A simple correlation for natural gas + condensate systems. *Fluid Phase Equilibria* **1986**, *29*, 383–390.

(18) Lee, S.-T.; Chien, M. A New Multicomponent Surface Tension Correlation Based on Scaling Theory. SPE/DOE Symposium on Enhanced Oil Recovery. Tulsa, 1984; pp 147–145.

(19) Danesh, A.; Dandekar, A.; Todd, A.; Sarkar, R. A Modified Scaling Law and Parachor Method Approach for Improved Prediction of Interfacial Tension of Gas-Condensate Systems. SPE Annual Technical Conference and Exhibition. Dallas, 1991; pp 515–523.

(20) Schechter, D. S.; Guo, B. Parachors Based on Modern Physics and Their Uses in IFT Prediction of Reservoir Fluids. *SPE* **1998**, *June*, 207–217.

(21) Defay, R.; Prigogine, I. *Surface tension and adsorption*; Wiley, 1966.

(22) Whitson, C. H.; Sunjerga, S. SPE 155499 PVT in Liquid-Rich Shale Reservoirs. SPE Annual Technical Conference and Exhibition. San Antonio, Texas, 2012; pp 8–10.

Graphical TOC Entry